The Canadian Mineralogist
Vol. 50, pp. 1453-1466 (2012)
DOI: 10.3749/canmin.50.6.1453

FLUORINE-RICH XENOTIME FROM THE WORLD-CLASS MADEIRA Nb–Ta–Sn DEPOSIT ASSOCIATED WITH THE ALBITE-ENRICHED GRANITE AT PITINGA, AMAZONIA, BRAZIL

ARTUR C. BASTOS NETO[§] AND VITOR P. PEREIRA

Instituto de Geociências, Universidade Federal do Rio Grande do Sul, Avenida Bento Gonçalves 950, CEP 91540-970, Porto Alegre, RS, Brazil

AMANDA C. PIRES

Instituto de Geociências, Universidade Federal de Roraima, Avenida Capitão Ene Garcez, 2413, CEP 69304-000, Boa Vista, RR, Brazil

LUC BARBANSON

ISTO, Université d'Orléans, Bâtiment Géosciences, rue de St. Amand, BP 6759, F–45067 Orléans, Cedex 2, France

ALAIN CHAUVET

MR5243, Géosciences, Université de Montpellier 2, Place Eugène Bataillon, F–34095 Montpellier, Cedex 5, France

ABSTRACT

The Madeira deposit (Sn, Nb, Ta) at Pitinga, Amazonia, in Brazil, is associated with the albite-enriched facies of the A-type Madeira granite (~1,820 Ma). Fluorine (cryolite), Y, REE, Li, Zr, and Th are potential by-products of the disseminated ore. We studied the xenotime from the core albite-enriched (CAG), transitional albite-enriched granite (TAG) and pegmatitic albite-enriched granite (PAG). In all these rocks, xenotime is magmatic, has high HREE contents (0.37 to 0.54 atoms per formula unit; LREE are not detected), and low U, Th and Ca content. The CAG xenotime is the richest in REE, followed by that in the PAG and TAG units. Fluorine was detected in all xenotime crystals from CAG (up to 5.10%) and from PAG (up to 1.40%) and in most crystals from TAG (up to 0.68%). Where the xenotime is richer in F, the Na and Si increase, the P, Ca, and the effectiveness of a thorite-type substitution decrease. Fluorine controls the ratio REE/Y; the richer the xenotime in F, the richer it is in REE, in particular Er and Yb. The cell parameters *a* and *c* are significantly shortened in F-rich xenotime. There is no evidence of OH in the structure. We contend that fluorine substitutes for O to form PO_3F tetrahedra, as in bobdownsite. The formation of the PO_3F tetrahedra in the xenotime accounts well for the compatibility between the crystallographic characteristics and the chemical composition.

Keywords: xenotime, yttrium, rare-earth elements, fluorine, albite-enriched granite, Pitinga, Amazonia, Brazil.

SOMMAIRE

Le gisement Madeira, situé dans le district minier de Pitinga, état de Amazonas, au Brésil, est associé au granite Madeira, de type A (~1820 Ma). Le gisement contient une association de Sn avec cryolite, Nb, Ta, Y, ETR, Li, Zr, U et Th dans le même granite, riche en albite, que celui qui encaisse un gisement de cryolite massive. Nous avons étudié le xénotime des sous-faciès granite à albite du coeur (GAC), granite à albite de transition (GAT) et granite à albite pegmatitique (GAP). Dans toutes ces roches, le xénotime est magmatique, et possède des teneurs élevées en terres rares (0,37 à 0,54 par formule unitaire; les terres rares légères n'ont pas été détectées) et des faibles teneurs en U, Th et Ca. Le xénotime de l'unité GAC est le plus riche en terres rares, suivi de ceux des unité GAP et GAT. Le fluor a été détecté dans tous les cristaux de xénotime du GAC (jusqu'à 5,10%) et du GAP (jusqu'à 1,40%) et dans la plupart des cristaux du GAT (jusqu'à 0,68%). Plus le xénotime est riche en F, plus les teneurs de Na, Si et P augmentent, et plus diminue l'efficacité de la substitution de type thorite. Le fluor contrôle le rapport de

§ *E-mail address*: artur.bastos@ufrgs.br

ETR/Y (plus le xénotime est riche en fluor, plus il est riche en terres rares, notamment Er et Yb). Les paramètres cristallins *a* et *c* sont sensiblement réduits dans le xénotime riche en F. Il n'existe aucune preuve de l'existence de OH dans la structure. Ceci est interprété en termes de substitution de O par F induisant la formation de tétraèdres PO_3F, tout comme dans la bobdownsite. La formation de ces tétraèdres dans le xénotime assure la compatibilité entre les caractéristiques cristallographiques et la composition chimique observées.

Mots-clés: xénotime, yttrium, terres rares, fluor, granite riche en albite, Pitinga, Amazonie, Brésil.

Introduction

China produces 97% of the rare-earth elements (REE) consumed in the world, but it is projected that by 2012, its national industry will consume the entire production, leaving the world dependent on the discovery of new reserves and leading to the increased use of known reserves (Stone 2009, Service 2010). The recovery of REE as a by-product will also become necessary. In this respect, the Madeira deposit, associated with the A-type Madeira granite at Pitinga, is among the world-class deposits with great potential.

This paper focuses on the xenotime found in the Madeira deposit. Xenotime has already been studied in detail in granites with the most diverse compositions; however, it has not been studied in the Madeira deposit, in which the association of cryolite with Sn, Nb, and Ta mineralization in an albite-enriched granite is unique in the world; furthermore, it presents an evolution marked by the enrichment in the heavy REE (HREE). As expected, the composition of the xenotime studied is also unique. We investigated the variations in the REE, Y, and F contents in xenotime of rocks formed from magma with different values of F fugacity (two different subfacies of the albite-enriched granite) and also in the presence of aqueous fluids rich in F (xenotime associated with pegmatitic albite-enriched granite). We also investigated the possible mechanisms of substitution that allow the incorporation of F into the structure of xenotime and the way in which such a process affects the structure of this mineral.

Background Information

Geological setting

The Pitinga region (Fig. 1) is located in the southern portion of the Guyana Shield (Almeida *et al.* 1981). The predominant rocks in the region are the volcanic rocks of the Iricoumé Group ($^{207}Pb/^{206}Pb$ zircon ages between 1,881 ± 2 and 1,890 ± 2 Ma). The rocks, indicative of a caldera complex, range from metaluminous to slightly peraluminous, demonstrate an affinity for the silica-saturated alkaline series or with A-type magmas (Ferron *et al.* 2002, 2006, 2010, Pierosan *et al.* 2011). The rocks of the Iricoumé Group are cross-cut by the granitic bodies of the Madeira Suite, among them the Madeira granite (Fig. 1).

A detailed description of the Madeira granite was provided by Costi *et al.* (2009). The Madeira granite (Figs. 1, 2) contains four facies (Costi 2000). The metaluminous amphibole–biotite syenogranite facies ($^{207}Pb/^{206}Pb$ zircon age of 1,824 ± 2 Ma: Costi *et al.* 2000) and the peraluminous biotite – alkali feldspar granite facies are equigranular. The alkali feldspar *hypersolvus* porphyritic granite facies ($^{207}Pb/^{206}Pb$ zircon age of 1,818 ± 2 Ma: Costi *et al.* 2000) and the albite-enriched granite were emplaced simultaneously and intrude the older facies. The albite-enriched granite is subdivided into two subfacies (Fig. 2), and the contact between them is gradational: the core albite-enriched granite (CAG) and the border albite-enriched granite (BAG). Locally, a transitional subfacies (TAG) can be identified.

The CAG is gray, with a porphyritic to seriate texture, and essentially consists of quartz, albite and K-feldspar in approximately equal proportions, each one ranging between 25 and 30%. Cryolite (5%), polylithionite (4%), green-brown mica (3%), zircon (2%), and blue amphibole (riebeckite, 2%) are accessory minerals. In minor proportions, we recognize pyrochlore, cassiterite, xenotime, thorite, and opaque mineral phases, such as magnetite and galena. Pegmatitic CAG, which has the same essential and accessory mineralogy, is usually rich in cryolite, xenotime, zircon and thorite; it occurs as lenses up to 1 m thick and is widespread throughout the CAG. The peraluminous BAG subfacies is red and presents the same textural types and essential mineralogy as the CAG except for the iron-rich minerals, *e.g.,* the Fe–Li mica, which have almost completely disappeared owing to an autometasomatic process (Costi 2000), and for the presence of fluorite instead of cryolite. Horbe *et al.* (1991) proposed that the albite-enriched granite is an "apogranite" and suggested a metasomatic model. Lenharo (1998) and Costi (2000) described the magmatic origin of the albite-enriched granite. Costi *et al.* (2009) proposed that the albite-rich granite originated through the crystallization of a dense, F-rich, peralkaline phase derived from a peralkaline to metaluminous parental melt by immiscibility.

The Madeira deposit

The term *Pitinga mine* is used to designate a mining complex, the main tin producer in Brazil, that comprises

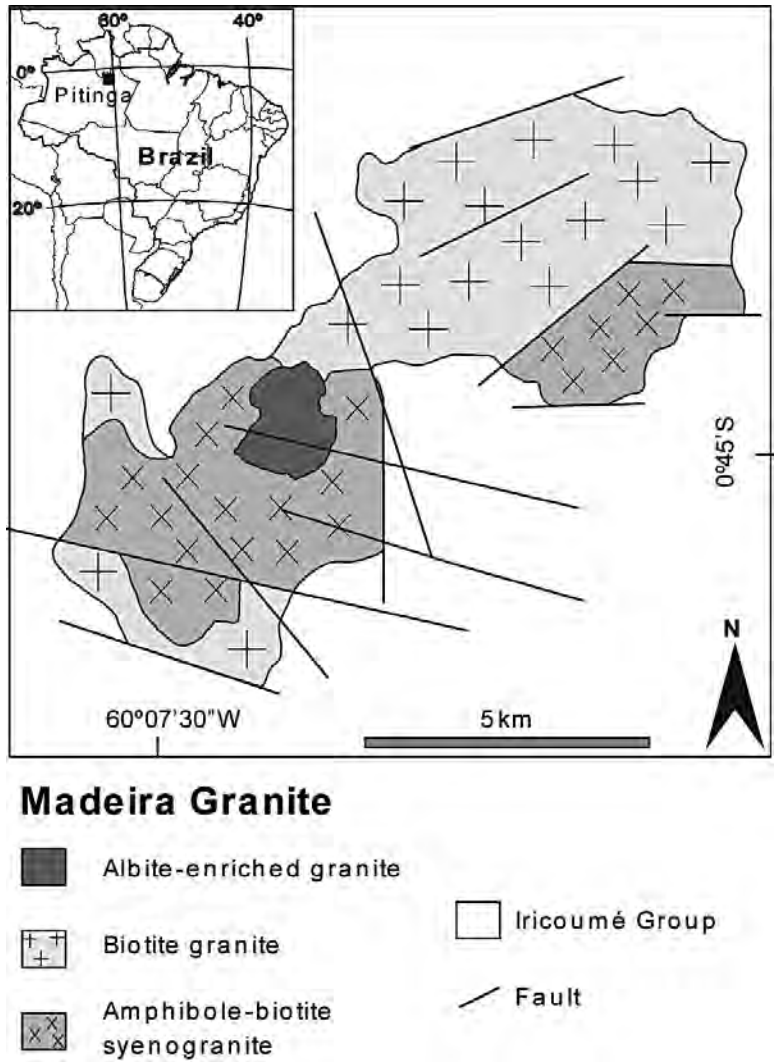

FIG. 1. Location map and geological map of the Madeira granite, modified after Costi (2000).

(1) alluvial deposits exploited since the 1980s, now almost exhausted, (2) greisens associated with the Água Boa granite (Madeira Suite) exploited between the years 1990 and 2000, and (3) the Madeira deposit, corresponding to the albite-enriched granite (Fig. 2), which was discovered by the Paranapanema Company in 1983 and is presently exploited for Sn, Nb and Ta.

The detailed description of the Madeira deposit was provided by Bastos Neto *et al.* (2005, 2009). The deposit has 164 million tonnes of disseminated ore at a grade of 0.17 wt% Sn (cassiterite), 0.20 wt% Nb_2O_5, 0.024 wt% Ta_2O_5 (both in pyrochlore and columbite), and 0.17 wt% REE [xenotime and gagarinite-(Y)]. Fluorine (cryolite), Zr (zircon), Th (thorite), and Li (polylithionite) are also potential by-products of the disseminated ore. In addition, in the central portion of the Madeira deposit, there is a massive cryolite deposit (MCD), amounting to 10 million tonnes with a grade of 31.9% Na_3AlF_6. In 2013, mining operations are expected to reach the MCD roof.

The Sn mineralization consists of magmatic cassiterite in both the CAG and the BAG. In the CAG, there are two types of disseminated cryolite. Cryolite I, magmatic, occurs as rounded crystals in the rock, as oval inclusions in quartz phenocrysts, and in mica agglomerates. Cryolite II, of a hydrothermal origin,

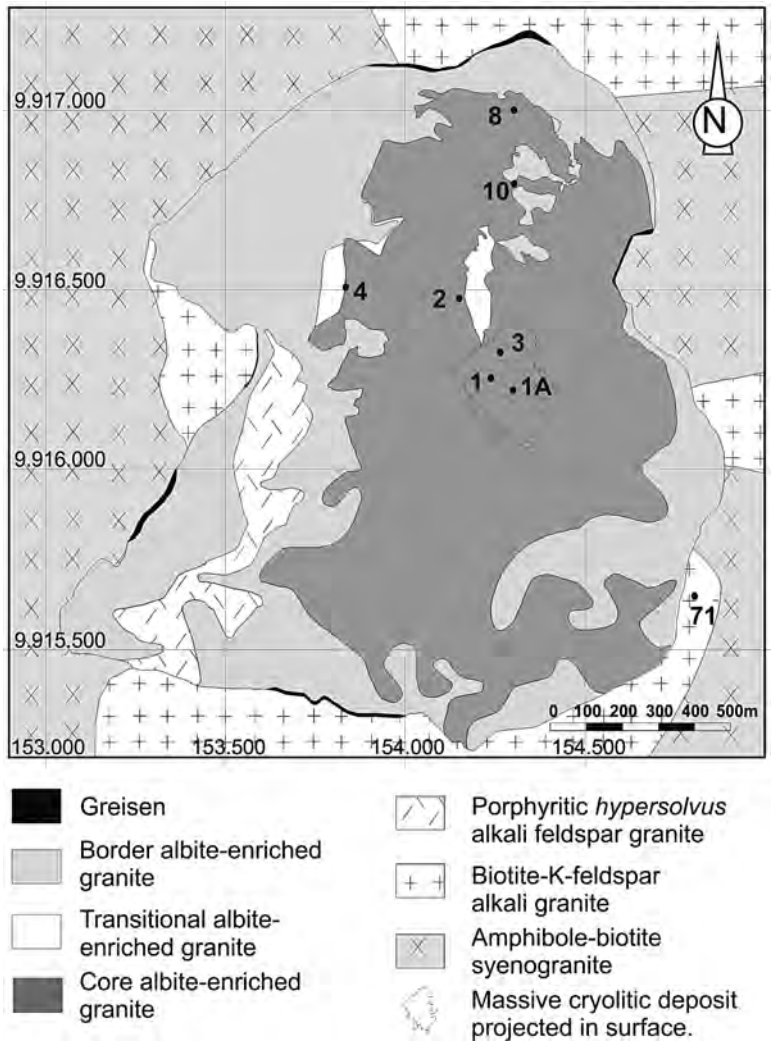

FIG. 2. Geological map of the albite-enriched granite facies (after Minuzzi *et al*. 2005a) and location of the samples.

occurs as a very finely disseminated (<0.05 mm) constituent in the rock matrix, corroding all minerals with which it is in contact. In the CAG and the BAG, the magmatic pyrochlore was affected by an alteration process characterized by a loss of Pb and an enrichment in U and Nb until its destabilization and the formation of columbite (Minuzzi *et al*. 2006a). The REE and Y disseminated mineralization is represented by xenotime (see below) and gagarinite-(Y) (Pires *et al*. 2006) that occurs only in the CAG intercalated in the lower portions of the massive cryolite deposit. These minerals contain fluocerite-(Ce) inclusions.

The MCD consists of several bodies of massive cryolite, intercalated with the CAG and hypersolvus granite; they are subhorizontal, up to 300 m long and up to 30 m thick, and made up of cryolite crystals (~87 vol.%), quartz, zircon, and feldspar (Minuzzi *et al*. 2006b). The REE and Y concentrations in the massive cryolite are very low (Y ≤ 20 ppm) (Minuzzi *et al*. 2008). The origin of the MCD is contentious. According to Lenharo (1998) and Costi (2000), the CAG evolved to a residual, extremely F-rich melt that formed the MCD. According to Bastos Neto *et al*. (2009), this extreme F enrichment is unlikely because

the F fugacity in the magma was buffered by the crystallization of cryolite I. The melt had a finite H_2O content, and the abrupt magmatic–hydrothermal transition triggered three processes: (a) cryolite II formation, (b) the alteration of pyrochlore, and (c) the formation of the MCD. The fluid-inclusion data on the massive cryolite (homogenization temperature between 100° and 400°C) attest to the hydrothermal origin of the MCD.

Xenotime

Xenotime, ideally YPO_4, is tetragonal, with space group $I4_1/amd$; it is isostructural with zircon (Ni *et al*. 1995). It is a common mineral in many geological environments and rock types, especially in granites, more particularly in Ca-depleted peraluminous granites. Xenotime has already been studied in detail in granites with the most diverse compositions (Thorpe *et al*. 1990, Miller *et al*. 1992, Ward *et al*. 1992, Casillas *et al*. 1995, Förster & Rhede 1995, Bea 1996). In the relevant magmas, xenotime is an early mineral responsible for the impoverishment of Y and HREE in the most differentiated facies (Wark & Miller 1993, Förster 1998). Xenotime is very stable (Broska *et al*. 2005) and has therefore been used in radiometric dating (Cocherie & Legendre 2007) and as a geothermometer (Andrehs & Heinrich 1998). Its content of trace elements provides important information on magmatic conditions (Kositcin *et al*. 2003).

Methods

Initially, we reviewed the available chemical data on the Madeira granite, aiming to define the potential of each facies for REE and Y. This led us to concentrate this work on the CAG. Almost two hundred CAG samples and thin sections have been re-examined. Sixty of them were selected for analysis with a scanning electron microscope, performed at UFRGS (JEOL, model JSM–5800); our objectives were to define the relationships between xenotime and the others minerals with REE (such as pyrochlore, zircon and thorite), to identify possible mineral inclusions, and to characterize its composition. The LREE were not detected in any of these samples. Eight CAG samples (Fig. 2) with xenotime were selected for analysis by electron microprobe (Cameca model SX 50) at the Bureau des Recherches Scientifiques et Minières, Orléans, France. The concentrations of P, Y, Si, U, Ca, Na, F, and HREE were determined with an accelerating voltage of 15 kV, a beam current of 20 nA and a focused beam. The concentrations of U, Th, and Pb were determined with an accelerating voltage of 30 kV and a beam current of 200 nA. Only the results with a significance level of 95% or more were retained.

Crystallographic studies were performed at UFRGS using the Siemens D5000 X-Ray Diffractometer (XRD) with a scanning step of 0.02°2θ, a time of 1 s, between 2 and 70°2θ, Co$K\alpha$ radiation and a nickel filter. The analyses by X-ray diffraction were pursued at the Institute des Sciences de la Terre d'Orléans, ISTO, France, with an INEL textural goniometer with a PSC 120 cobalt tube and a XRG 3000 generator. The analyses were performed on thin sections, using a current of 35 nA and an acceleration voltage of 30 kV. The inclination angles were $\omega = 5$, $\Psi = 0°$ to 80°, with a step of 2.5° and, over the range 0–355°, with a step of 5°. The acquisition time for each point was 10 s; the total time for each thin section was 8 h. Crystallographic parameters were determined by Least-squares Refinement of Crystallographic Lattice Parameters (LCLSQ 8.5 software, Burnham 1993). The analysis by infrared spectroscopy were performed at UFRGS using the Perkin–Elmer Fourier-transform spectrometer over the range 400 to 4000 cm^{-1}. The Raman analyses were performed at the Laboratoire de Spectrométrie Raman (BRGM–CNRS) à Orléans, France, by J.-M. Beny (ISTO–CNRS).

Results: Xenotime Distribution and Relationships with Other REE and Y-Bearing Minerals

In the CAG, xenotime is magmatic, occurring as crystals scattered in the rock matrix, as inclusions in minerals or arranged interstitially, reaching 0.5% (by vol.). The crystals range in size between 0.05 and 0.44 mm; they are subhedral to euhedral and form short (Fig. 3A) or elongate prisms (Figs. 3B, C). Mineral inclusions were not observed in xenotime, but BSE images allowed us to identify abundant thorite and pyrochlore inclusions, which are both subhedral from 5 to 10 μm (Fig. 3G), in zircon associated with the xenotime. The xenotime in TAG also is magmatic and subhedral to euhedral (Fig. 3D), but the prisms are both more elongate (up to 0.3 cm) and more abundant (up to 3% by vol.) than in CAG. Pyrochlore grains in CAG and TAG are brown, yellow or caramel, subhedral or less commonly euhedral, from 0.07 to 0.41 mm across; they occur mainly in the interstices of albite or accessory minerals or are enclosed in quartz and feldspar. An earlier zircon exists as very small crystals, up to 0.1 mm, anhedral, more commonly included in quartz phenocrysts. A later zircon is more abundant, more commonly euhedral to subhedral, 0.1 to 1 mm in size, with inclusions of albite, cryolite and opaque phases. Thorite occurs as fine crystals, up to 0.5 mm, within the rock matrix. In summary, the petrographic and SEM analysis showed that in the CAG and TAG, the crystallization of xenotime was preceded by the crystallization of pyrochlore and early zircon, and was synchronous with thorite and partially synchronous with the late generation of zircon.

In the pegmatitic CAG (Figs. 3E, F), xenotime occurs as brown prismatic crystals, 4 cm long by 0.5 cm in width. It may constitute up to 30% (by vol.), and is associated principally with orthoclase, polylithionite,

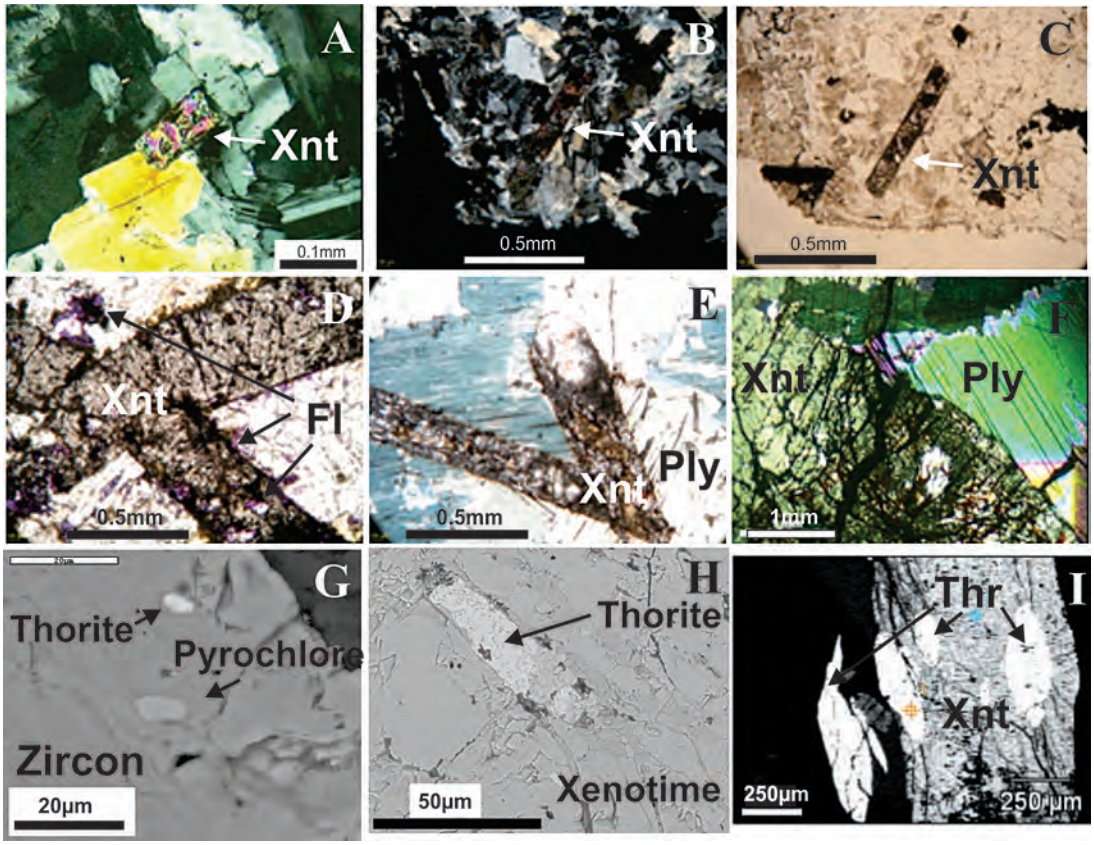

FIG. 3. Photomicrographs and SEM images of xenotime from the albite-enriched granite. A, B and C. Typical xenotime of the core albite-enriched granite matrix (A: short prism, PL; B: elongate prism, PL; C, same elongate prism, NL). D. Xenotime and secondary fluorite from the transitional albite-enriched granite, NL. E. Xenotime and polylithionite from the pegmatitic albite-enriched granite, NL. F. Xenotime, with fractures (black) filled by thorite and iron oxides, and polylithionite, from the pegmatitic albite-enriched granite, PL. G. BSE image of pyrochlore and thorite inclusions in zircon associated with xenotime in the core albite-enriched granite. H. BSE image of the inclusion of prismatic thorite in xenotime from the pegmatitic core albite-enriched granite. I. BSE image of xenotime from the pegmatitic albite-enriched granite with oval inclusions of thorite. Abbreviations: Xnt: xenotime, Thr: thorite, Ply: polylithionite, Fl: fluorite, NL: natural light transmitted, PL: polarized light.

cryolite, and quartz phenocrysts. Thorite may form well-developed crystals up to 4 cm across. Xenotime contains thorite inclusions reaching 20 μm. These inclusions display two habits: (i) prismatic outlined crystal (Fig. 3H) which are clearly older than xenotime, or (ii) an irregular or oval shape (Fig. 3I); in this case, the relationships with xenotime are complex. In the crystals of xenotime hosting irregular or oval inclusions of thorite, microveinlets (Fig. 3I) are found to be filled with a material containing F, Y, Ca and REE and iron oxide released from the destabilization of thorite. These microveinlets are 50 μm in length by approximately 2 μm thick and are restricted to xenotime.

THE COMPOSITION OF XENOTIME

Table 1 presents representative compositions of xenotime from the border and middle part of the CAG, pegmatitic CAG and the TAG. The analysis of the disseminated xenotime in the central part of the CAG are not of high quality owing to poor totals related to hydrothermal alteration. Because of the presence of high amounts of F, two F-rich xenotime crystals were analyzed with infrared spectroscopy to evaluate the existence of structural OH. The infrared spectra present peaks at 974, 642, 542 and 440 cm^{-1}. There is no evidence of OH in the xenotime structure. Two Raman spectra were obtained from each of the crystals, one parallel and one perpendicular to the elongation of

the crystal. The spectra are similar to those observed in common xenotime (http://rruff.info). As no evidence of the presence of the OH group was detected, structural formulas were calculated with the following assumptions: the sum of cations equal to 2 atoms, (*i.e.,* site VIII + site IV = 2), and the amount of oxygen was calculated by subtracting the fluoride content (*i.e.,* O = 4 – F).

In this article, yttrium is not included among the REE. The HREE patterns in all grains and the enclosing rocks are very similar (Fig. 4). The disseminated xenotime in CAG is the richest in REE (Fig. 5a). The chemical composition of xenotime does not present systematic variations related to the location of the sample in the CAG. Because Sc was not detected, the composition in terms of end members is xenotime-$(Y)_{50}$ and xenotime-$(HREE)_{50}$. The value of P in the structural formula is a little less than 1 in 80% of the analyses and, in many of these cases, even after the addition of Si, vacancies remain at the tetrahedral site, especially in the compositions with more F. Part of these cases may be linked to the accuracy of the analysis of P (0.9%). Thorium, Na and Si were detected in small amounts in all cases. Fluorine was detected in all grains, with concentrations ranging from 0.5% to 4.7%. Relationships between the amount of F and some of the other elements are quite obvious: the more F there is in

TABLE 1. REPRESENTATIVE COMPOSITIONS OF XENOTIME FROM ALBITE-ENRICHED GRANITE

	Core albite-enriched granite						Pegmatitic albite-enriched granite						Transitional albite-enriched granite			
sample	8			10			1		3				71			
analysis	43	45	47	50	53	75	6	16	76	60	61	78	21	28	57	58
P_2O_5 wt%	28.84	28.88	30.17	30.19	29.4	30.2	32.49	31.99	32.14	33.24	32.82	32.14	32.59	32.82	33.19	33.15
SiO_2	0.23	0.35	0.22	0.12	0.26	0.19	0.05	0.04	0.02	0.01	0.03	0.03	b.d.l.	0.02	0.15	0.14
Y_2O_3	24.35	23.69	23.4	23.21	24.75	25.26	27.25	26.83	26.98	28.05	29.07	28.13	31.16	31.09	27.97	27.68
Gd_2O_3	4.24	3.62	4.95	3.92	4.21	4.08	4.16	4.40	4.07	3.73	3.65	3.90	2.91	2.93	3.09	4.14
Dy_2O_3	7.08	7.47	7.86	7.66	7.63	6.25	7.47	7.54	7.77	6.21	6.31	6.09	4.61	5.68	6.09	7.42
Ho_2O_3	2.16	2.74	2.94	2.39	2.53	2.00	2.71	2.63	2.80	2.13	2.27	2.01	1.56	2.21	2.19	2.25
Er_2O_3	10.51	10.64	11.96	11.84	11.22	9.57	9.72	10.49	9.93	9.59	9.29	9.51	8.25	8.23	11.16	10.68
Yb_2O_3	16.04	15.72	15.23	15.73	14.11	17.64	13.41	14.25	14.07	15.24	14.78	15.06	14.14	12.96	15.12	14.38
Lu_2O_3	1.70	1.56	1.49	1.95	2.02	2.08	1.39	1.45	1.34	1.80	1.62	1.83	2.29	1.95	1.70	1.55
CaO	0.03	0.27	b.d.l.	0.04	0.03	b.d.l.	0.03	0.04	b.d.l.	0.05	0.01	b.d.l.	b.d.l.	0.06	0.03	0.03
Na_2O	0.06	0.08	0.03	0.03	0.14	0.05	0.03	b.d.l.	b.d.l.	b.d.l.	0.01	b.d.l.	0.02	0.02	0.04	0.02
ThO_2	0.65	1.28	0.39	0.09	1.14	0.37	0.04	0.29	0.11	0.13	0.39	0.09	b.d.l.	0.01	0.1	0.43
UO_2	b.d.l.	b.d.l.	b.d.l.	b.d.l.	b.d.l.	b.d.l.	0.04	b.d.l.	b.d.l.	b.d.l.	b.d.l.	b.d.l.	b.d.l.	b.d.l.	0.04	b.d.l.
F	4.03	4.00	2.46	2.74	4.70	3.04	0.81	1.07	1.40	0.64	0.87	0.85	b.d.l.	0.68	0.54	0.16
Total	99.91	100.30	101.09	99.90	102.12	100.70	99.60	101.00	100.62	100.82	101.12	99.63	97.53	98.67	101.38	102.04
F=O	1.7	1.69	1.04	1.15	1.98	1.28	0.34	0.45	0.59	0.27	0.37	0.36	b.d.l.	0.29	0.23	0.07
Total	98.22	98.61	100.06	98.75	100.14	99.44	99.26	100.6	100.03	100.55	100.76	99.28	97.53	98.38	101.16	101.97
P *apfu*	0.950	0.952	0.968	0.979	0.950	0.968	1.003	0.989	0.996	1.010	0.997	0.994	1.008	1.009	1.003	0.998
Si	0.009	0.014	0.008	0.005	0.010	0.007	0.002	0.001	0.001	b.d.l.	0.001	0.001	b.d.l.	0.001	0.005	0.005
Y	0.505	0.491	0.472	0.473	0.503	0.509	0.529	0.522	0.525	0.536	0.555	0.547	0.606	0.601	0.531	0.524
Gd	0.055	0.047	0.062	0.05	0.053	0.051	0.050	0.053	0.049	0.044	0.043	0.047	0.035	0.035	0.037	0.049
Dy	0.089	0.094	0.096	0.095	0.094	0.076	0.088	0.089	0.092	0.072	0.073	0.072	0.054	0.066	0.070	0.085
Ho	0.027	0.034	0.035	0.029	0.031	0.024	0.031	0.031	0.033	0.024	0.026	0.023	0.018	0.026	0.025	0.025
Er	0.128	0.130	0.142	0.143	0.135	0.114	0.111	0.12	0.114	0.108	0.105	0.109	0.095	0.094	0.125	0.119
Yb	0.190	0.187	0.176	0.184	0.164	0.204	0.149	0.159	0.157	0.167	0.162	0.168	0.157	0.143	0.164	0.156
Lu	0.020	0.018	0.017	0.023	0.023	0.024	0.015	0.016	0.015	0.020	0.018	0.020	0.025	0.021	0.018	0.017
Ca	0.017	0.017	0.017	0.017	0.017	0.017	0.018	0.018	0.018	0.018	0.018	0.018	0	0.002	0.018	0.018
Na	0.005	0.006	0.002	0.003	0.010	0.004	0.002	b.d.l.	b.d.l.	b.d.l.	b.d.l.	b.d.l.	b.d.l.	0.001	0.002	0.002
Th	0.006	0.011	0.003	0.001	0.010	0.003	b.d.l.	0.002	0.001	0.001	0.003	0.001	b.d.l.	b.d.l.	0.001	0.003
U	b.d.l.	b.d.l.	b.d.l.	b.d.l.	b.d.l.	b.d.l.	b.d.l.	b.d.l.	b.d.l.	b.d.l.	b.d.l.	b.d.l.	b.d.l.	b.d.l.	b.d.l.	b.d.l.
F	0.496	0.493	0.295	0.332	0.568	0.364	0.094	0.124	0.161	0.073	0.099	0.098	b.d.l.	0.078	0.060	0.018
O	3.504	3.507	3.705	3.668	3.432	3.636	3.906	3.876	3.839	3.927	3.901	3.902	4.000	3.922	3.940	3.982

b.d.l.: below detection limit.

xenotime, the less P (Fig. 5b) and the more Si and Na. Calcium, although it occurs at very low concentrations, presents a strong negative correlation with F (Fig. 5c). The correlation coefficient between F and P is –0.94. The correlation coefficient between Si and P, –0.64, is lower than expected for elements that supposedly replace each another. A positive correlation (+0.80) between Si and Th was also observed (Fig. 5d).

The xenotime from pegmatitic CAG is systematically slightly enriched in Y on the border of the crystals. The composition in terms of the end members is xenotime-$(Y)_{54}$ and xenotime-$(HREE)_{46}$. The xenotime typically contains less REE than the CAG xenotime (Fig. 5a). The content of P is greater than that of the CAG xenotime; calculated vacancies at the tetrahedral site are less common (50% of the analysis) and fewer. Thorium and Si occur in concentrations from very low to the highest among the studied samples of xenotime (Fig. 5d) and with a more significant correlation (+0.89) than in the CAG xenotime. Fluorine was detected in all cases, with concentrations of 0.5% to 1.9%. The relationship between the F and other elements are as discussed earlier.

The xenotime of TAG was analyzed in one rock sample only, in which all the xenotime crystals are texturally similar, although it apparently has two types of xenotime that are distinguishable on the basis of their Y content (Fig. 5a). In both types of xenotime, there is no vacancy at the tetrahedral site, the level of incorporation of Ca, Na, and Th at the site of Y is quite limited, and P and Si show a negative correlation (–0.76) that is better than that found in the xenotime of CAG. Fluorine was detected in most of the cases, with concentrations of up to 0.7%, which is consistently lower than those found in the xenotime from CAG and from pegmatitic CAG, but can still be considered high for this mineral.

The Lattice Parameters of Xenotime

The lattice parameters *a* and *c* of xenotime were determined in well-developed F-rich crystals from the pegmatitic CAG (Table 2).

The *c* and *a* parameters of YPO_4 are, respectively, shorter than in $TbPO_4$ and $DyPO_4$, and greater than in $HoPO_4$, $ErPO_4$, $TmPO_4$, $YbPO_4$, and $LuPO_4$ (Fig. 6a). They accurately reflect the differences in the atomic radius of the occupant of the octahedral site. The *c* and *a* parameters of natural xenotime (Ni *et al*. 1995, Mogilevsky *et al*. 2006, Demartin *et al*. 1991) have, respectively, dimensions close to those of YPO_4, as

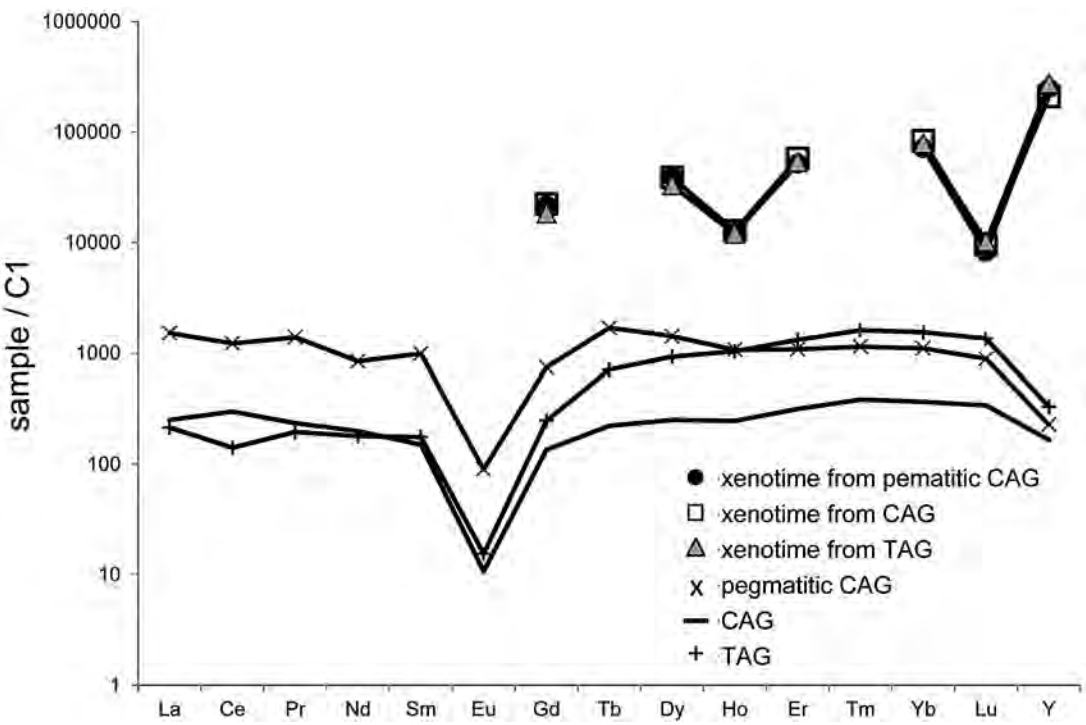

FIG. 4. Patterns of rare-earth-element distribution (normalized to chondrite C1 (Anders & Grevesse 1989) in xenotime (analysis with an electronic microprobe, this work) and albite-enriched granite (analyses by ICP–MS, in Pires 2010).

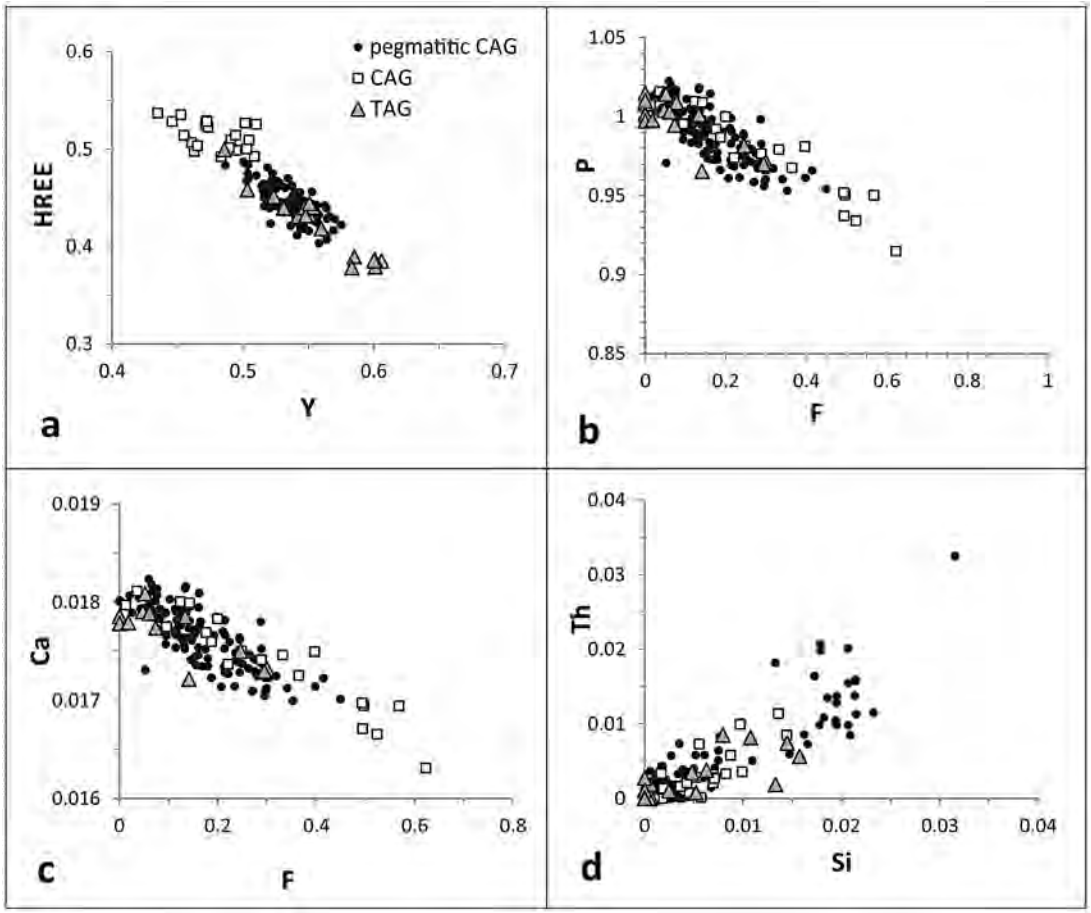

FIG. 5. Binary diagrams for xenotime from albite-enriched granite. (a) Y *versus* HREE, (b) F *versus* P, (c) F *versus* Ca, (d) Si *versus* Th. Concentrations are expressed in *apfu*. CAG: core albite-enriched granite; TAG: transitional albite-enriched granite.

the two examples shown (Fig. 6a). The xenotime from the pegmatitic CAG has the shortest *c* and *a* parameters among all natural samples of xenotime (Fig. 6a). Overall, this is consistent with the total REE content and especially with the predominance of Yb and Er. However, the shortening of both *c* and *a* parameters is much greater than expected. They also seem to have been modified to different extents. Consequently, the *c* and *a* parameters are likely affected by a factor other than the replacement of Y by REE. This additional factor would seem to be related to the replacement of O by F.

These parameters (Table 2) allowed the calculations of unit-cell volume and density using the average structural formula of the xenotime from the pegmatitic CAG. The volume is slightly lower than that of other natural xenotime. The density is significantly greater than that of other samples of the mineral. This is likely related to the combination of two factors: the smaller volume of its unit cell and the highest REE content, which are elements that are heavier than Y.

DISCUSSION

In comparison with xenotime as described in the literature (Vainshtein *et al*. 1956, Åmli & Griffin 1975, Sabourdy *et al*. 1997, Demartin *et al*. 1991, Franz *et al*. 1996, Masau *et al*. 2000, Asami *et al*. 2002, Broska *et al*. 2005, Mogilevsky *et al*. 2006, among others), the xenotime from the Madeira deposit is distinguished by six main characteristics: (1) it is among the richest in F, (2) the crystals have no zoning in F and in other elements, (3) it is among the richest in HREE, (4) it does not contain LREE (most HREE-enriched xenotime contains at least 2 wt% of LREE), (5) the contents of U, Th, and Ca are very low, and (6) the ratio U/Th is less

than 1 (most xenotime from other locations have U/Th values greater than 1).

The xenotime of the Madeira deposit shows some chemical similarities with that described by Förster (1998) in Li-rich mica-bearing peraluminous Ca-poor A-type granite. Both have very high contents of HREE, have a Y/Ho value lower than that of chondrite, a U/Th value less than 1, and F in the structure. However, in the Madeira xenotime, the concentration of actinides and Ca is much smaller. According to Förster (1998), the xenotime formed by the breakdown of zircon or thorite, or both, which would explain the high contents of the HREE. In the CAG, despite the early appearance of thorite, the textures observed in the SEM images show that the destabilization of thorite observed in xenotime cannot explain the formation of xenotime. In the pegmatitic CAG, the complex relationships between thorite and xenotime and between thorite and zircon require further detailed investigation.

A cheralitic [$CaTh(PO_4)_2$] substitution, found in xenotime at other locations (Franz *et al.* 1996, Förster 1998), does not occur in the Madeira deposit. The ratio U/Th, less than 1 in xenotime from the Madeira deposit, differs from that of xenotime from other locations, which incorporates more U than Th in its crystal structure (Demartin *et al.* 1991, Franz *et al.* 1996, Sabourdy *et al.* 1997, Asami *et al.* 2002, Broska *et al.* 2005), mainly in the presence of monazite. Its structure better accommodates Th, whereas the xenotime structure better accommodates U, owing to differences in ionic radius (Förster 1998). However, the CAG is more enriched in Th than in U and does not contain monazite.

In the xenotime from the Madeira deposit, the relationships between F and some of the other elements are quite obvious: where the xenotime is richer in F, the (REE,Y), Na, and Si increase, and it is poorer in P and Ca. There is no vacancy at the tetrahedral site where the F concentration is less than ~0.8%; above this value, the richer the xenotime is in F, the higher the vacancy at the tetrahedral site. Fluorine must also exercise control over REE/Y: the richer xenotime is in F, the richer it is in REE. The relationship found between Si and Th, as well as the presence of Si, may be explained by a thorite-type substitution, $Y^{3+} + P^{5+} = Th^{4+} + Si^{4+}$ (Förster 1998). However, the effectiveness of this substitution is greater if the F content in xenotime is lower (see the values of the correlation between Si and Th), and the correlation coefficient between Si and P (–0.64) is lower than expected for elements that supposedly replace each other. As we will see, the control is likely exercised by the changes that fluorine causes in the xenotime structure.

The positive correlation between F and Si leads to the assumption that F can replace O in the Si-bearing tetrahedra, following the substitution $O^{2-} + P^{5+} = F^{1-} +$

TABLE 2. CRYSTALLOGRAPHIC PARAMETERS OF XENOTIME FROM THE PEGMATITIC ALBITE-ENRICHED GRANITE AND FROM NOVO HORIZONTE

	Sample 2	σ	Novo Horizonte*
a (Å)	6.884	0.007	6.8982
c (Å)	6.009	0.012	6.037
V (Å³)	284.752	0.711	287.271
Calculated density (g/cm³)	5.146		4.658

* Mogilevsky *et al.* (2006).

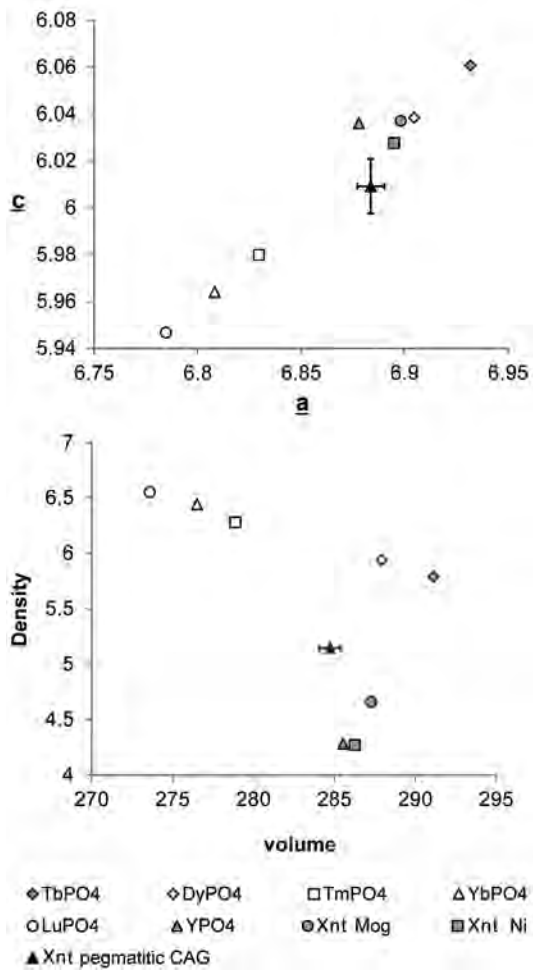

FIG. 6. Crystallographic parameters of xenotime from the pegmatitic albite-enriched granite compared with other samples of xenotime and synthetic compounds. A. Unit-cell parameters *a versus c*. B. Unit-cell volume *versus* density. Data on synthetic compounds are taken from Ni *et al.* (1995). Xnt Ni: xenotime (natural) in Ni *et al.* (1995). Xnt Mog: xenotime (natural) in Mogilevsky *et al.* (2006).

Si^{4+}). However, the concentration of Si is very low, so that this mechanism alone cannot explain such an enrichment in F in xenotime. Larger amounts of F could be incorporated by a mechanism similar to that described in F-rich hydro-grossular, $\{\square(F,OH)_4\}^{4-} = \{SiO_4\}^{4-}$ (Valley *et al*. 1983, Barbanson & Bastos Neto 1992). However, this mechanism involves an increase in the unit-cell size (Smyth *et al*. 1990), so its application to the PO_4 tetrahedra in the xenotime from the Madeira deposit is unlikely. It follows, therefore, that the formation of the PO_3F tetrahedra must be considered.

The presence of PO_3F tetrahedra has already been identified in several synthetic compounds, for instance, $Cu(H_2O)_2(NH_4)_2(PO_3F)_2$ (Berraho *et al*. 1994), but it was only recently found in nature. Bobdownsite (Tait *et al*. 2011), ideally $Ca_9Mg(PO_4)_6(PO_3F)$, is a new mineral species from the Big Fish River, Yukon, Canada. Bobdownsite is isotypic with whitlockite $Ca_9Mg(PO_4)_6(PO_3OH)$. The relationship between the fluorine content and the cell parameters in bobdownsite–whitlockite solid-solution series indicates that the halogen causes a shortening in both the *a* and the *c* parameters, mainly in the former.

The formation of the PO_3F tetrahedra in the xenotime from the Madeira deposit allows for the compatibility between the crystallographic characteristics and the chemical composition. As this substitution causes a decrease in volume and, consequently, a greater difficulty in accepting larger cations, an F-rich xenotime would preferentially incorporate Er and Yb (both REE with an ionic radius smaller than Y) at the expense of Y. This is exactly what occurs in the Madeira deposit. Furthermore, the incorporation of LREE would be virtually impossible. In xenotime with minor amounts of F, the balance of the electrostatic charge appears to have been obtained through the substitution $O^{2-} + P^{5+} = F^{1-} + Si^{4+}$. However, in the xenotime with major amount of F, there is not much Si. A possible explanation is that the contraction of the unit cell hampers the replacement of P (0.17 Å) by Si (0.26Å). This explains the strong correlation between P and F (–0.94), the weak correlation between P and Si (–0.64), the poor effectiveness of a thorite-type substitution in F-rich xenotime, and vacancies at the P site in order to achieve the balance of electrostatic charges.

The crystallization of pyrochlore in CAG had begun prior to xenotime crystallization. The pyrochlore contains significant amounts of LREE and also U and Th (Minuzzi *et al*. 2006a, Bastos Neto *et al*. 2009). Thus, we believe that the paucity of U and Th in the xenotime is partially due to this, but other factors could be involved. The early appearance of pyrochlore in F-rich magmas that formed granites with disseminated cryolite was already described in the Kaffo Valley albite arfvedsonite granite, Ririwai Complex, one of the Younger Granites of Nigeria (Ogunleye *et al*. 2006). Moreover, the crystallization of pyrochlore instead of columbite (which may not contain as much U as pyrochlore) is also related to the richness of the system in fluorine (Linnen & Keppler 1997).

As observed by Bastos Neto *et al*. (2009) and in agreement with the experimental data of Dolejš & Baker (2007), the CAG did not evolve to an extremely F-enriched magma because the F content of the magma was buffered by cryolite crystallization. This determined the character of the Nb and Sn mineralization, which is homogeneously dispersed in the CAG, and it is very likely that the REE, which are also transported by magmatic F-bearing complexes, were in the same way homogeneously dispersed in the CAG, resulting in some features found in xenotime, such as high F contents regardless of the position in the CAG, and the lack of significant zonation in crystals.

Conclusions

Our study of xenotime associated with the Madeira deposit led to the following conclusions:

1) The xenotime is magmatic in all the varieties of the albite-enriched granite studied. It is characterized by high REE contents (0.37 to 0.56 atoms per formula unit). The xenotime from the CAG is the richest in REE, followed by xenotime from the pegmatitic CAG and from the TAG. The HREE patterns in all varieties of xenotime are very similar to each other and in relation to the respective rocks. The LREE are not present in the structure. The contents of the actinides U and Th and of Ca are relatively very low. The positive correlation between Si and Th indicates the occurrence of a thorite substitution.

2) The fluorine concentration in xenotime reflects the fugacity of fluorine in the environment. In the CAG xenotime, F is present in all crystals and usually with high concentrations, up to 5.10%. In the pegmatitic CAG, F is invariably present, but the concentrations are typically lower than those in CAG. The xenotime from TAG typically either presents lower F concentrations or it is not present.

3) The presence of fluorine in the structure of xenotime caused the shortening of both parameters *a* and *c*, which were modified in different proportions. The calculated unit-cell volume of the F-rich xenotime is lower than that usually encountered. There is no OH in the structure. We contend that fluorine substitutes for O, forming PO_3F tetrahedra, as in bobdownsite (Tait *et al*. 2011), in which the halogen causes a shortening in both the *a* and *c* parameters in different proportions.

4) The formation of the PO_3F tetrahedra in xenotime explains the compatibility between its crystallographic characteristics and the chemical composition. As this substitution causes a decrease in volume and, consequently, a greater difficulty in accepting larger cations, the F-rich xenotime preferentially incorporates Er and Yb at the expense of Y, and the incorporation of LREE is virtually impossible. The shrinkage of the unit cell likely hampers the replacement of P by Si, and this

explains other chemical features, such as the good correlation between P and F, the weak correlation between P and Si, and the lower effectiveness of the thorite-type substitution in F-rich xenotime.

Acknowledgements

Xenotime is one of the accessories commonly encountered in pegmatitic associations. The authors are pleased to contribute this article about the cristal-chemical characteristics of F-rich xenotime to an issue dedicated to Petr Černý. In doing so, we recognize his important role in the world of granitic pegmatites, and his guidance in understanding these complex associations.

The authors thank the Agência para o Desenvolvimento Tecnológico da Indústria Mineral do Brasil (ADIMB), the Departamento Nacional da Produção Mineral (DNPM), the Financiadora de Estudos e Projetos (FINEP), the Conselho Nacional de Desenvolvimento Científico e Tecnológico (CNPq), and the CTMINERAL for financial support, and thank the Mineração Taboca S.A. for supporting the field work. Thanks are also due to Drs. Robert F. Martin, Daniel Ohnenstetter, and Gerhard Franz, whose comments and criticisms have greatly improved the manuscript.

References

Almeida, F.F.M., Hasuy, Y., Brito Neves, B.B. de & Fuck, R.A. (1981): Brazilian structural provinces: an introduction. *Earth-Sci. Rev.* **17**, 1-29.

Åmli, R. & Griffin, W.L. (1975): Microprobe analysis of REE minerals using empirical correction factors. *Am. Mineral.* **60**, 599-606.

Anders, E. & Grevesse, N. (1989): Abundances of elements: meteoritic and solar. *Geochim. Cosmochim. Acta* **53**, 197-214.

Andrehs, G. & Heinrich, W. (1998): Experimental determination of REE distributions between monazite and xenotime: potential for temperature-calibrated geochronology. *Chem. Geol.* **149**, 83-96.

Asami, M., Suzuki, K. & Grew, E.S. (2002): Chemical Th–U–total Pb dating by electron microprobe analysis of monazite, xenotime and zircon from the Archean Napier Complex, East Antarctica: evidence for ultra-high-temperature metamorphism at 2400 Ma. *Precamb. Res.* **114**, 249-275.

Barbanson, L. & Bastos Neto, A.C. (1992): Hydroandradite titanifère fluorée et grenat ($Spe_{39}Gro_{33}Alm_{23}And_6$) fluoré des granitoïdes du district à fluorine de Santa Catarina (Brésil): déscription minéralogique, mécanisme d'incorporation du fluor, signification pétrologique et métallogénique. *C.R. Acad. Sci. Paris, sér.* II, **314**(2), 63-69.

Bastos Neto, A.C., Pereira, V.P., Lima, E.F., Ferron, J.M., Minuzzi, O., Ronchi, L.H., Flores, J.A.A., Frantz, J.C., Pires, A.C., Pierosan, R., Hoff, R., Botelho, N.F., Rolim, S.B.A., Rocha, F.N.F. & Ulmann, L. (2005): The cryolite ore deposit, Pitinga mine (Amazonas). *In* Ore Mineral Deposits from Amazonian Mining Districts (J.O. Marini, E. Queiroz & B.W. Ramos, eds.). DNPM- ADIMB, Brazilia, Brazil (477-552; in Portuguese).

Bastos Neto, A.C., Pereira, V.P., Ronchi, L.H., de Lima, E.F. & Frantz, J.C. (2009): The world-class Sn, Nb, Ta, F (Y, REE, Li) deposit and the massive cryolite deposit associated with the albite-enriched facies of the Madeira A-type granite, Pitinga mining district, Amazonas State, Brazil. *Can. Mineral.* **47**, 1329-1357.

Bea, F. (1996): Residence of REE, Y, Th and U in granites and crustal protoliths: implications for chemistry of crustal melts. *J. Petrol.* **37**, 521-552.

Berraho, M., Vegas, A., Martínez-Ripoll, M. & Rafiq, M. (1994): A copper monofluorophosphate, $Cu(H_2O)_2(NH_4)_2(PO_3F)_2$. *Acta Crystallogr.* **C50**, 666-668.

Broska, I., Williams, C.T., Janák, M. & Nagy, G. (2005): Alteration and breakdown of xenotime-(Y) and monazite-(Ce) in granitic rocks of the Western Carpathians, Slovakia. *Lithos* **82**, 71-83.

Burnham, C.W. (1993): Least-squares refinement of crystallographic lattice parameters. Harvard Univ., Cambridge, Massachusetts.

Casillas, R., Nagy, G., Pantó, G., Brändle, J. & Fórizs, I. (1995): Ocurrence of Th, U, Y, Zr and REE-bearing accessory minerals in late-Variscan granitic rocks from the Sierra de Guadarrama (Spain). *Eur. J. Mineral.* **7**, 989-1006.

Cocherie, A. & Legendre, O. (2007): Potential minerals for determining U–Th–Pb chemical age using electron microprobe. *Lithos* **93**, 288-309.

Costi, H.T. (2000): *Petrology of Rare Metals-, High-F Alkaline Granites: the Example of the Albite Granite from the Pitinga Mine, Amazonas State, Brazil*. Doctoral thesis, Federal University of Pará, Belém, Brazil (in Portuguese).

Costi, H.T., Dall'Agnol, R. & Moura, C.A.V. (2000): Geology and Pb–Pb geochronology of Paleoproterozoic volcanic and granitic rocks of Pitinga province, Amazonian Craton, Northern Brazil. *Int. Geol. Rev.* **42**, 832-849.

Costi, H.T., Dall'Agnol, R., Pichavant, M. & Rämö, O.T. (2009): The peralkaline tin-mineralized Madeira cryolite albite-rich granite of Pitinga, Amazonian Craton, Brazil: petrography, mineralogy and crystallization processes. *Can. Mineral.* **47**, 1301-1327.

Demartin, F., Pilati, T., Diella, V., Donzelli, S., Gentille, P. & Gramaccioli, C.M. (1991): The chemical composition of xenotime from fissures and pegmatites in Alps. *Can. Mineral.* **29**, 69-75.

DOLEJŠ, D. & BAKER, D.R. (2007): Liquidus equilibria in the system K_2O–Na_2O–Al_2O_3–SiO_2–F_2O_{-1}–H_2O to 100 MPa. II. Differentiation paths of fluorosilicic magmas in hydrous systems. *J. Petrol.* **48**, 807-828.

FERRON, J.M.T.M., BASTOS NETO, A.C., LIMA, E.F., COSTI, H.T., MOURA, C., PRADO, M. & GALARZA, M. (2006): Geology and Pb–Pb geochronology of granitic and volcanic acid to intermediate Paleoproterozoic rocks from the Pitinga province, Amazonian craton. *Revista Brasileira de Geociências* **36**, 499-512 (in Portuguese).

FERRON, J.M.T.M., BASTOS NETO, A.C., LIMA, E.F., NARDI, L.V.S., COSTI, H.T., PIEROSAN, R. & PRADO, M. (2010): Petrology, geochemistry, and geochronology of Paleoproterozoic volcanic and granitic rocks (1.89 to 1.88 Ga) of the Pitinga province, Amazonian Craton, Brazil. *J. S. Am. Earth Sci.* **29**, 483-497.

FERRON, J.M.T.M., BASTOS NETO, A.C., ROLIM, S.B.A., HOFF, R., UMANN, L.V. & MINUZZI, O.R.R. (2002): Recognition of a mega-structure in the Pitinga mining district (Amazonas State): preliminary data from the application of techniques of digital processing of Landsat 7 ETM+ images. *In* 2nd Symposium on Volcanism (Belém), (in Portuguese).

FÖRSTER, H.-J. (1998): The chemical composition of REE–Y–Th–U-rich accessory minerals in peraluminous granites of Erzgebirge–Fichtelgebirge region, Germany. II. Xenotime. *Am. Mineral.* **83**, 1302-1315.

FÖRSTER, H.-J. & RHEDE, D. (1995): Composition of monazite and xenotime from the Fichtelgebirge granites – an electron microprobe study. *Ber. Deutsch. Mineral. Ges., Eur. J. Mineral.* **7**, 68 (abstr.).

FRANZ, G., ANDREHS, G. & RHEDE, D. (1996): Crystal chemistry of monazite and xenotime from Saxothuringian-Moldanubian metapelites, NE Bavaria, Germany. *Eur. J. Mineral.* **8**, 1097-1118.

HORBE, M.A., HORBE, A.C., COSTI, H.T. & TEIXEIRA, J.T. (1991): Geochemical characteristics of cryolite – tin-bearing granites from the Pitinga mine, northwestern Brazil – a review. *J. Geochem. Explor.* **40**, 227-249.

KOSITCIN, N., MCNAUGHTON, N.J., GRIFFIN, B.J., FLETCHER, I., GROVES, D.I. & RASMUSSEN, B. (2003): Textural and geochemical discrimination between xenotime of different origin in the Archaean Witwatersrand Basin, South Africa. *Geochim. Cosmochim. Acta* **67**, 709-731.

LENHARO, S.L.R. (1998): *Magmatic Evolution and Metallogenetic Model of the Mineralized Granites from the Pitinga Region, Amazonas State, Brazil.* Doctoral thesis, Univ. of São Paulo, São Paulo, Brazil (in Portuguese).

LINNEN, R.L. & KEPPLER, H. (1997): Columbite solubility in granitic melts: consequences for the enrichment and fractionation of Nb and Ta in the Earth's crust. *Contrib. Mineral. Petrol.* **128**, 213-227.

MASAU, M., ČERNÝ, P. & CHAPMAN, R. (2000): Dysprosian xenotime-(Y) from the Annie Claim #3 granitic pegmatite, southeastern Manitoba, Canada: evidence of the tetrad effect? *Can. Mineral.* **38**, 899-905.

MILLER, C.F., HANCHAR, J.M., WOODEN, J.L., BENNETT, V.C., HARRISON, T.M., WARK, D.A. & FOSTER, D.A. (1992): Source region of a granite batholith: evidence from lower crustal xenoliths and inherited accessory minerals. *Trans. R. Soc. Edinburgh, Earth Sci.* **83**, 49-62.

MINUZZI, O.R.R., BASTOS NETO, A.C., FORMOSO, M.L.L., ANDRADE, S., JANASI, V. & FLORES, J.A.A. (2008): Rare earth element and yttrium geochemistry applied to the genetic study of cryolite ore at the Pitinga mine (Amazon, Brazil). *Anais da Academia Brasileira de Ciências* **80**, 719-733.

MINUZZI, O.R.R., BASTOS NETO, A.C., PEREIRA, V.P. & FLORES, J.A.A. (2006b): The massive cryolite deposit and the disseminated ore of cryolite from the Pitinga mine (Amazonas State, Brazil). *Revista Brasileira de Geociências* **36**, 104-123.

MINUZZI, O.R.R., BASTOS NETO, A.C., PEREIRA, V.P. & NUNES, L. (2006a): Pyrochlore columbitization in the albite-enriched granite from the Pitinga mine (Amazonas State): relationship with the cryolite mineralization. *Revista Brasileira de Geociências* **36**, 124-137.

MOGILEVSKY, P., ZARETSKY, E. B., PARTHASARATHY, T. A. & MEISENKOTHEN, F. (2006): Composition, lattice parameters, and room temperature elastic constants of natural single crystal xenotime from Novo Horizonte. *Phys. Chem. Minerals* **33**, 691-698.

NI, YUNXIANG, HUGUES, J.M. & MARIANO, A.N. (1995): Crystal chemistry of monazite and xenotime structures. *Am. Mineral.* **80**, 21-26.

OGUNLEYE, P.O., GARBA, I. & IKE, E.C. (2006): Factors contributing to enrichment and crystallization of niobium in pyrochlore in the Kaffo albite arfvedsonite granite, Ririwai Complex, Younger Granites province of Nigeria. *J. Afr. Earth Sci.* **44**, 372-382.

PIEROSAN, R., LIMA, E.F., NARDI, L.V.S., BASTOS NETO, A.C., CAMPOS, C.P., FERRON, J.M.T.M. & PRADO, M. (2011): Geochemistry of Palaeoproterozoic volcanic rocks of the Iricoume Group, Pitinga Mining District, Amazonian craton, Brazil. *Int. Geol. Rev.* **53**, 946-976.

PIRES, A.C. (2010): *Xenotima, gagarinita, fluocerita e waimirita da mina Pitinga (AM): mineralogia e avaliação preliminar do potencial do albita granito para exploração de elementos terras raras e ítrio.* Doctoral thesis, Federal University of Rio Grande do Sul, Porto Alegre, Brazil.

PIRES, A.C., BASTOS NETO, A.C., PEREIRA, V.P., BOTELHO, N.F. & MINUZZI, O.R.R. (2006): Gagarinita-(Y) with fluocerite polymorphous: probable case of formation of a new mineral by LREE exsolution from HREE fluoride (Pitinga mine, Amazonas State). *Revista Brasileira de Geociências* **36**, 155-164 (in Portuguese).

SABOURDY, G., SAGON, J.-P. & PASTIER, P. (1997): La composition chimique du xénotime en Limousin, Massif Central, France. *Can. Mineral.* **35**, 937-946.

SERVICE, R.F. (2010): Nations move to head off shortages of rare earths. *Science* **26**(327), 1596-1597.

SMYTH, J.R., MADEL, R.E., MCCORMICK, T.C., MUNOZ, J.L. & ROSSMAN, G.R. (1990): Crystal-structure refinement of a F-bearing spessartine garnet. *Am. Mineral.* **75**, 314-318.

STONE, R. (2009): As China's rare earth R&D becomes ever more rarefied, others tremble. *Science* **325**, 1336-1337.

TAIT, K.T., BARKLEY, M.C., THOMPSON, R.M., ORIGLIERI, S., EVANS, S.H., PREWITT, C.T. & YANG, HEXIONG (2011): Bobdownsite, a new mineral from Big Fish River, Yukon, Canada, and its structural relationship with whitelockite-type compounds. *Can. Mineral.* **49**, 1065-1078.

THORPE, R.S., TINDLE, A.G. & GLEDHILL, A. (1990): The petrology and origin of the Tertiary Lundy granite (Bristol Channel, UK). *J. Petrol.* **31**, 1379-1406.

VAINSHTEIN, E.E., TUGARINOV, A.I. & TURANSKAYA, N.V. (1956): Regularities in the distribution of rare earth in certain minerals. *Geokhimiya* **1**, 36-56.

VALLEY, J.W., ESSENE, E.J. & PEACOR, D.R. (1983): Fluorine-bearing garnets in Adirondack calc-silicates. *Am. Mineral.* **68**, 444-448.

WARD, C.D., MCARTHUR, J.M. & WALSH, J.N. (1992): Rare earth element behavior during evolution and alteration of the Dartmoor granite, SW England. *J. Petrol.* **33**, 785-815.

WARK, D.A. & MILLER, C.F. (1993): Accessory mineral behavior during differentiation of a granite suite: monazite, xenotime and zircon in the Sweetwater Wash pluton, southeastern California, U.S.A. *Chem. Geol.* **110**, 49-67.

Received May 19, 2011, revised manuscript accepted September 5, 2012.